Article

Modelling of Resistive Type Superconducting Fault Current Limiter for HVDC Grids

Guillermo García [1], D. Marene Larruskain [2],* and Agurtzane Etxegarai [2]

[1] Ingeteam Power Technology, 48170 Zamudio, Spain; guillermopla.95@gmail.com
[2] Department of Electrical Engineering, Faculty of Engineering of Bilbao, University of the Basque Country UPV/EHU, 48013 Bilbao, Spain; agurtzane.etxegarai@ehu.eus
*   Correspondence: marene.larruskain@ehu.eus

Abstract: The protection of high voltage direct current (HVDC) grids is a challenge considering that the protection system must detect, locate, and interrupt large fault currents in a few milliseconds. Resistive type superconducting fault current limiters (R-SFCL) can help solve that difficult task, reducing the extremely demanding ratings of HVDC circuit breakers. This paper presents different approaches to model R-SFCLs in order to analyze their suitability for assessing the performance of HVDC grid protection, including the step model, the exponential model, the RQ model, and the magneto-thermal model. In the first instance, the R-SFCL models are evaluated in a test grid to analyze their parameterisation and select the most adequate model for the study of HVDC grids. The RQ model is finally chosen for its simplicity but closer behavior to the magneto thermal model in terms of fault resistance dependency and resistance evolution curve. Then, the performance of an RQ type R-SFCL model in conjunction with a mechanical circuit breaker is evaluated in a multiterminal HVDC grid with different fault cases. This way, fault currents are greatly decreased as well as circuit breaker requirements. Hence, the R-SFCL under study enables a reliable protection of the HVDC grid.

Keywords: HVDC grid; fault current limiter; model; resistive type; superconductivity

1. Introduction

High voltage direct current (HVDC) grids are considered a key solution for the reinforcement of the power system, to integrate large scale renewable energies and to cope with the increase in electrical energy demand. Nevertheless, HVDC technology is not mature enough to enable the wide existence of these grids, and most of the HVDC transmissions installed currently are two-point systems. One of the most demanding features is fault clearance, since DC currents have no natural zero crossing, which makes it difficult for HVDC circuit breakers (DCCB) to operate. Furthermore, converters are highly sensitive to large fault currents that arise shortly after fault inception [1]. Therefore, protection of HVDC grids against DC faults is a major challenge for the development of future HVDC grids in order to ensure safe and stable operation.

Traditionally, point-to-point HVDC systems have been protected by tripping breakers on the AC side. However, this can lead to the full de-energisation of the grid, which makes this alternative unreliable for HVDC grids [2], especially when it comes to overhead lines [3]. Consequently, the requirements for DCCBs are highly demanding, since they must interrupt large fault currents within a few milliseconds, while in AC systems they operate in several AC cycles [2]. Therefore, DCCBs are still under development and commercial models have emerged very recently at huge expenses.

With this in mind, fault current limiters (FCLs), which both limit rise rate and peak value of fault currents, are of concern for the protection of HVDC grids. FCLs are devices with virtually zero impedance during normal system operation, but when a fault occurs, the impedance of the devices increases to the set value [4]. The resistance of the superconducting materials modulates as a function of current and temperature.

FCLs are applicable in any segment of the power system, including generation, transmission, and distribution [5,6]. Nevertheless, higher voltage levels constitute a hurdle that limits the employment of FCLs on account of the required voltage insulation. Occasionally, there are a few projects for 220 kV applications. Within this context, the 220 kV and 1200 A rated resistive superconducting fault current limiter (R-SFCL) which is installed in a substation in Moscow stands out [7].

FCL applications in power systems include the assistance with the penetration of distributed generation. This way, distributed generators can be connected to the power grid without increasing short circuit levels. Besides FCLs can facilitate the meshed operation, given that in the event of a fault they can control the fault currents in the faulty parts of the feeder and isolate the affected segments. Other applications include bus splitting, compliance with N-1 criteria by ruling out costly elements, neutral connection without permanent impedance drawbacks, subgrid coupling avoiding sequential tripping, busbar coupling and transformer feeder, power plant auxiliaries, and ship propulsion systems [5,6]. Lastly, SFCLs can be practical for protecting HVDC systems. The increase in impedance results in a reduction in fault current, which makes it easier to operate DCCBs. Consequently, the highly demanding requirements of DCCBs are reduced and lower-rated DCCBs are feasible.

Among the different types of FCLs, various researchers have claimed that the R-SFCL is a promising solution for the protection of HVDC grids [8–14]. The main advantages of R-SFCL are their applicability to high voltage and currents, high reliability, low harmonics, very small losses, and low voltage drops. These characteristics make them appropriate for high voltage power systems, such as HVDC and more specifically, for modular multilevel converter (MMC)-based HVDC systems.

Several types of R-SFCL simulation models can be found in the literature with different transient responses compared to the empirical performance of superconductors [15].

Zero-dimensional approaches employ time-dependent resistances without thermal estimates. These simplified methods include binary models that operate at an specific time [16] or in function of the current magnitude [17]. Therefore, they are able to reduce fault currents but they do not exhibit the required period of time for heating and developing resistance. Non-linear look-up tables adjust this limitation and gradually state the resistance [18]. Some models represent the recovery time [19].

One-dimensional models consider heat diffusion in one dimension (length or thickness) and uniform temperature across other dimensions. Likewise, nonhomogenous critical currents are taken into account. These models can be fairly accurate in cases of large fault currents with homogeneus heating. The authors of [20] studied the transference of heat to the coolant and the abrupt temperature variations that decrease the thermal transfer efficiency. In [21], the non-uniformity of temperature and the so-called hot spots are analyzed, as well as the effect of the current on the temperature distribution. The effect of the tape length in hot spots is analyzed in [22].

Classical magneto-thermal analysis involves complex calculations that require long simulation times to produce accurate models. Therefore, some authors use simplified magneto-thermal models, based on empirical results [23–25]. Simplified and magneto-thermal models have been developed by simulation tools including ATP/EMTP, PSCAD/EMTDC, and MATLAB/Simulink.

Finite element methods (FEM) deal with two- and three-dimensional symmetries that consider heat diffusion along two or three dimensions of the tape, respectively [26–28]. FEMs develop top accuracy models at the expense of very long simulation times, which are difficult to combine with HVDC grids analysis. On account of the time consuming methodology, FEM models are regularly used for the validation of other models [29].

For the evaluation of HVDC systems, simplified or magneto-thermal models with different levels of complexity and, therefore, accuracy, are regularly used. For greater thermal or electromagnetic accuracy, FEM models are applied. Therefore, a consensus must be reached between the model accuracy and the required simulation time.

Most papers analyze the design of R-SFCLs from the equipment perspective [8]; nonetheless, this paper focuses on the system performance perspective. In this way, the paper presents different approaches to model R-SFCLs, with the application of HVDC grid protection. The rest of the paper is organized as follows: in Section 3, the models under study are applied in a test grid and their respective performances are discussed. Based on the previous discussion, Section 4 analyzes the performance of an R-SFCL with the most adequate model in a HVDC grid under different fault case scenarios. Finally, the main conclusions are outlined.

2. Modelling of R-SFCL

An R-SFCL consists of a layered superconducting tape structure and a shunt resistance that decreases over-voltages during quenching and diverts part of the fault current after the quench, with the purpose of avoiding overheating [30]. That resistance can be external and/or bonded to the superconductor. However, it is frequently omitted to simplify the analysis [29,30]. For electrical power system simulations purposes, the R-SFCL can be modeled as a zero dimensional variable resistor with constant critical current density distribution.

The operation of the R-SFCL can be differentiated into three states. In the superconducting state, the temperature (T) and current (I) are below their respective critical values (T_C and I_C), as shown in Equation (1). In this state, the R-SFCL exhibits no resistance.

$$T < T_c \qquad I < I_C \tag{1}$$

In the typically denominated flux-flow state, the critical current, related to the critical current density J_C, is surpassed as shown in Equation (2). The device develops resistance on account of the temperature increase.

$$T < T_c \qquad I > I_C \tag{2}$$

The R-SFCL operates in the normal conducting state when the temperature and current are over their critical values, Equation (3). At this state, the device shows resistance. The change from superconducting to normal state is called quench.

$$T > T_C \qquad I > I_C \tag{3}$$

After this state, the R-SFCLs might require a restoration period for cooling and returning to the superconducting state.

The thermal behavior of the R-SFCL is modeled as in [31], where the model assumes a constant thermal coefficient to cooling reservoir. These assumptions have a small impact in electrical behavior as stated in [32]. The constant critical current density distribution ensures uniform temperature evolution along the tape. This way, the generated heat is calculated in Equation (4)

$$\dot{Q}_{gen} = R_{SFCL} \cdot I^2 \tag{4}$$

On the other hand, the removed heat by the cooling system is shown in Equation (5).

$$Q_{Removed} = \frac{T - Ta}{R_{th_{SC}}} \tag{5}$$

where T and T_a are the instantaneous temperatures of device and ambient, respectively, and $R_{th_{SC}}$ is the thermal resistance of the superconductor. This thermal resistance can generally be calculated as in Equation (6).

$$R_{th_{SC}} = \frac{1}{k \cdot L \cdot D \cdot \pi} \tag{6}$$

where k is the thermal conductivity.

The temperature gradient can be calculated as in Equation (7).

$$\frac{dT}{dt} = \frac{Q_{R_{SFCL}} - Q_{removed}}{C_{sc}} \tag{7}$$

where C_{sc} is the superconductor thermal capacity, which is calculated as in Equation (8).

$$C_{sc} = L \cdot D \cdot \pi \cdot C_v \tag{8}$$

where C_v is the superconductor volumetric specific heat.

Several R-SFCL models have been developed in the literature [15]. The choice of the model mainly depends on the desired accuracy, which must be in compromize with computational cost.

Generally, the R-SFCL models that are used for the analysis of HVDC grids can be distinguished into four groups: step model, exponential model, RQ model, and magneto-thermal model. There are also more accurate models with high computational costs which are usually not feasible for such studies.

2.1. Step Model

The step model is the simplest one, which is based on a binary model that takes the superconducting and normal conducting states into consideration, as shown in Equation (9),

$$\left| R_{SFCL}(t) = 0 \;|i(t)| < i_C \quad R_{SFCL}(t) = R_{MAX} \;|i(t)| > i_C \;\right| \tag{9}$$

where R_{MAX} is the developed maximum resistance and i_C is the critical current.

As soon as the circulating current surpasses the critical current, the model instantaneously develops the maximum resistance value, resulting in a square curve. Thus, no peak current analysis can be performed. This model is far away from the real behavior of an R-SFCL, but it is still used for its simplicity and adequacy for steady state analysis.

2.2. Exponential Model

The exponential model is a widely recognized model based on a binary model with a transition time for emulating the flux-flow state is given by Equation (10).

$$\left| R_{SFCL} = 0 \;|i(t)| < i_C \quad R_{SFCL} = R_{MAX} \cdot \left(1 - e^{\frac{t_o - t}{\tau}}\right) \;|i(t)| > i_C \;\right| \tag{10}$$

where t_o is the fault inception time.

The delay of the transition enables peak current analysis whilst it maintains simplicity. Normal conducting state to superconducting state transition can be modeled with a slope.

Figure 1 shows a comparison of the step model and exponential model curves with and without recovery [15].

2.3. RQ Model

The RQ model is based on the empirically observed dependence between the generated heat (Q) and the developed resistance of the SFCL (R) independently of the current value. In [29,33], empirical RQ curves are obtained for a YBCO tape. These types of curves can be implemented in look-up-tables for emulating the quenching phenomena of the SFCL, as shown in Figure 2.

2.4. Magneto-Thermal Model

The magneto-thermal model is the most complex and accurate model used in the analysis of HVDC grids. The model is based on the relation between the electric field and current density (E-J characteristic) of high temperature superconducting (HTS) materials (Figure 3), which shows a non-linear relation between current density and electric field [34]. It considers the dependence of the temperature in the electrical variables.
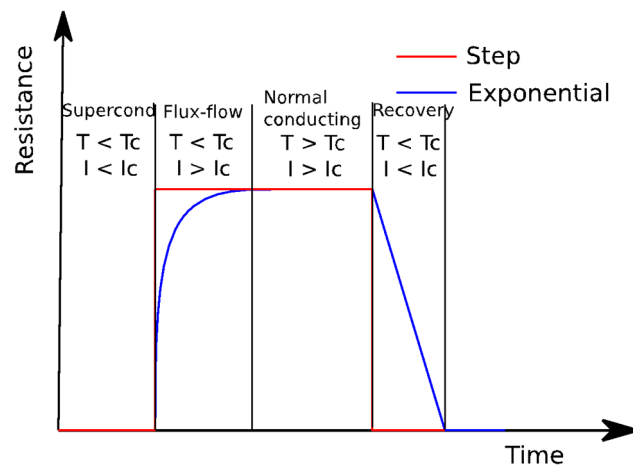
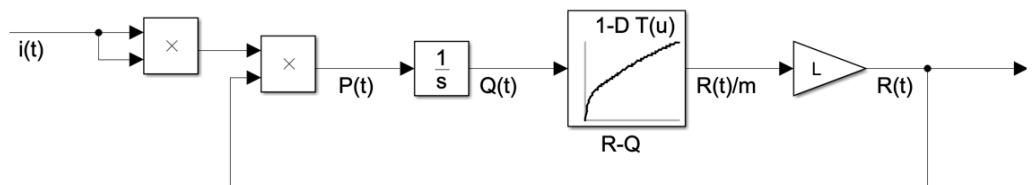**Figure 1.** Step and exponential model comparison.

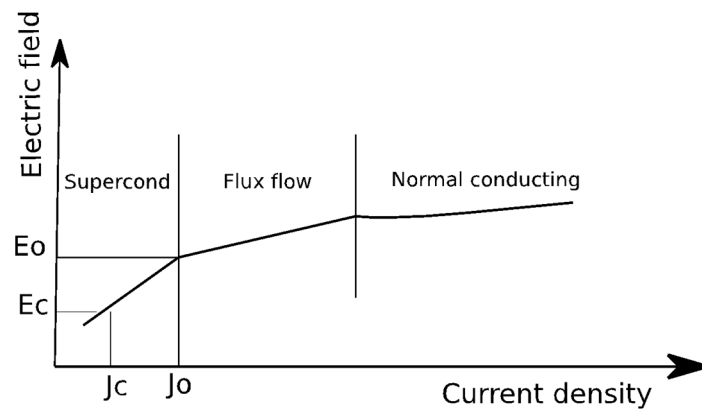**Figure 2.** Block diagram of RQ Model.

Figure 3. E-J characteristic of HTS material.

This model distinguishes with reasonable accuracy the three states of the superconductor.

1. Superconducting state: when current density (J) is low enough, the electric field (E) and resistive value are negligible as shown in Equations (11) and (12).

$$E(J,T) = E_C \left[\frac{J}{J_C(T)} \right]^{\alpha} \tag{11}$$

$$J_C(T) = J_C(77K) \left[\frac{(T_C - T)}{(T_C - 77)^{1.8}} \right] \tag{12}$$

where α is a quenching constant.

2. Flux-flow state: the device starts developing some electric field and resistive value Equation (13).

$$E(J,T) = E_o \left(\frac{E_C}{E_o} \right)^{\left(\frac{\beta}{\alpha} \right)} \frac{J_C(77K)}{J_C(T)} \left(\frac{J}{J_C(77K)} \right)^{\beta} \tag{13}$$

where β, E_o and E_C are the second quenching constant, critical electric field, and electric field constant, respectively.

For superconducting and flux-flow states, instantaneous resistivity (ρ) can be calculated as in Equation (14).

$$\rho = \frac{J(t)}{E(t)} \tag{14}$$

3. Normal conducting state: the device behaves as a resistor and the relation between electric field and current density is linear, Equations (15) and (16).

$$E(J,T) = \rho(T_c)\frac{T}{T_C}J \tag{15}$$

$$\rho(T) = \rho(T_c)\frac{T}{T_C} \tag{16}$$

where ρ is the resistivity of the material in normal conducting state.

Normal state resistance is calculated in Equation (17).

$$R = \rho(T)\frac{L}{D\pi} \tag{17}$$

where L and D are the superconductor length and diameter.

The three stages of the magneto-thermal model are shown in Figure 3 and implemented with algorithms in the flow chart depicted in Figure 4.
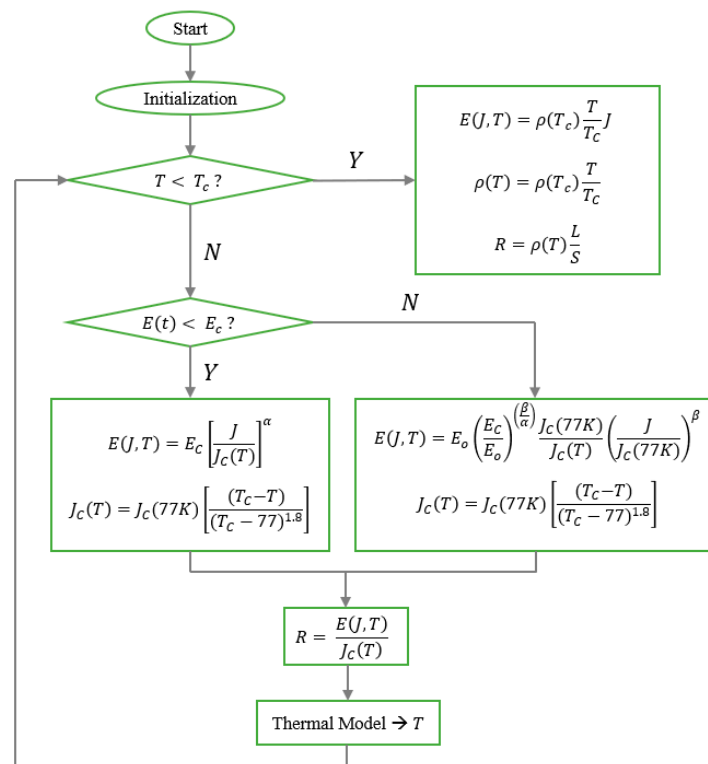

Figure 4. Magneto-Thermal model flow chart.

3. Test Grid and Model Analysis

In this section the four R-SFCL models under study are implemented in MATLAB/Simulink and tested in the simplified DC test bed depicted in Figure 5.
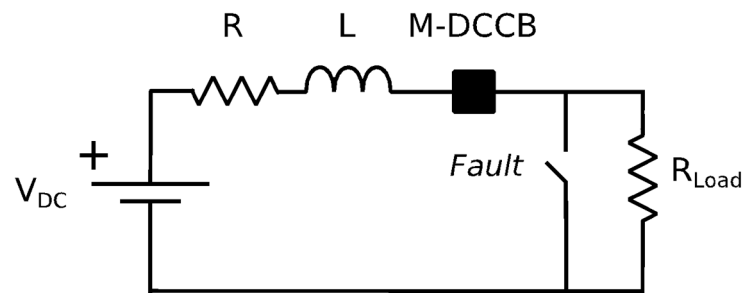
Figure 5. Simplified DC test bed.

The parameters of the test grid are shown in Table 1.

Table 1. Test grid parameters.

Variable	Value	Unit
U_{dc}	100	[kV]
L_{line}	50	[mH]
R_{line}	5	[Ω]
R_{load}	500	[Ω]
R_{fault}	5	[Ω]
t_{fault}	0.05	[s]
$I_{prospective}$	10	[kA]

One of the advantages of the implementation of a SFCL in a HVDC grid is that a slower and less costly DCCB can be employed as a higher fault interruption time does not imply higher fault current values [12]. Thus, in the paper, the mechanical active current injection DCCB (M-DCCB) shown in Figure 6 is implemented to clear the fault. The parameters of the M-DCCB are shown in Table 2.
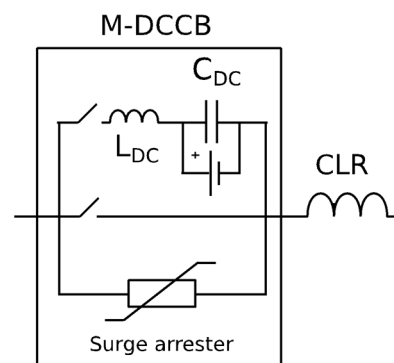

Figure 6. Implemented Active Injection M-DCCB.

Table 2. Implemented M-DCCB parameters.

Variable	Value	Unit
L_{dc}	290	[uH]
C_{dc}	17.7	[uF]
L_{CLR}	1	[mH]
$V_{SurgeArrester}$	1.5	pu
I_c	4	[kA]
$M-DCCB_{Operation\ delay}$	17	[ms]

Furthermore, the response of the models defined in Section 2 are analyzed for diverse model settings values and different fault resistance scenarios, which are common in the literature.

3.1. Step Model

The step model is simulated with a 30 Ω final resistance value. Figure 7 depicts the fault current and R-SFCL resistance. It can be appreciated how this model is not appropriate for the analysis of peak currents since the current value fluctuates straight away between steady state and fault case values.
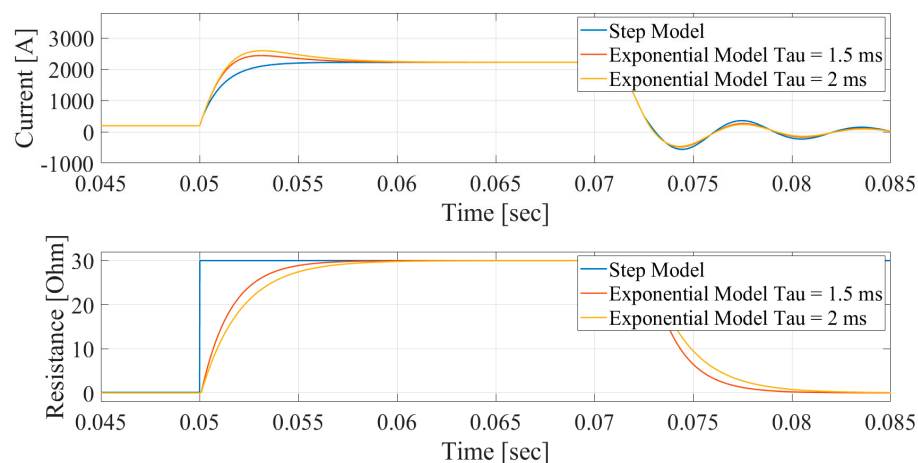

Figure 7. Step Model and Exponential Model analysis for different transition time values.

3.2. Exponential Model

The exponential model is implemented in the test bed for 30 Ω final resistance value and two transition times, τ, i.e., 1.5 and 2 ms. Figure 7 shows fault current and R-SFCL resistance for the different time constants. Large time constant results in higger peak currents.

An adequate R-SFCL design should limit both peak and steady state fault currents. Thus, it can be concluded that it is important to have a fast transition time compared to the system response (electrical time constant of the faulted circuit). Therefore, the transition time of the R-SFCL should be fixed considering the possible circuit time constants.

Finally, in step and exponential models, fault resistance variations have no impact on transition time, as is justified in Section 2.2.

3.3. RQ Model

In this section, the model diagram of Figure 2 is implemented in the test bed together with the look-up table that contains the R-Q relation of [31]. The superconducting tape consists of a YBCO layer, combined with copper, silver, stainless steel, and Hastelloy substrate layers. The final R-SFCL resistance is 30 Ω and three tape lengths, 400, 600, and 800 m, have been considered.

Figure 8 shows fault current and resistance evolution of RQ model for the different tape lengths. For larger lengths, the final resistive value is developed faster. Thus, the modification of tape length adjusts the desired transition time that defines the peak current.

Besides, Figure 9 shows the influence of fault resistance in the transition time of the RQ model for 5, 10, and 15 Ω fault cases. An interesting characteristic of this model is that quenching phenomenon slows down for higger fault resistances. This makes sense since the increase in fault resistances reduces the current across the R-SFCL. Hence, the heat-resistance development slows down. This behavior is not to be seen with the previous two models.
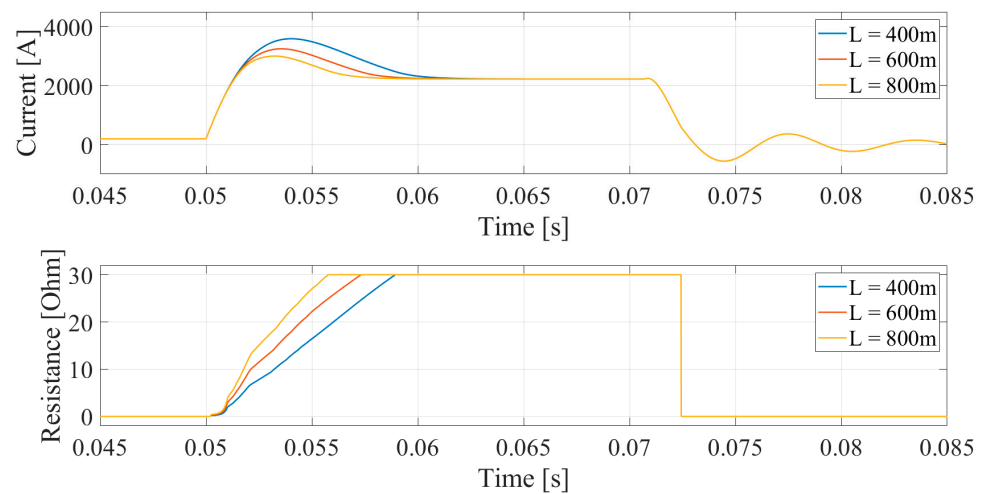
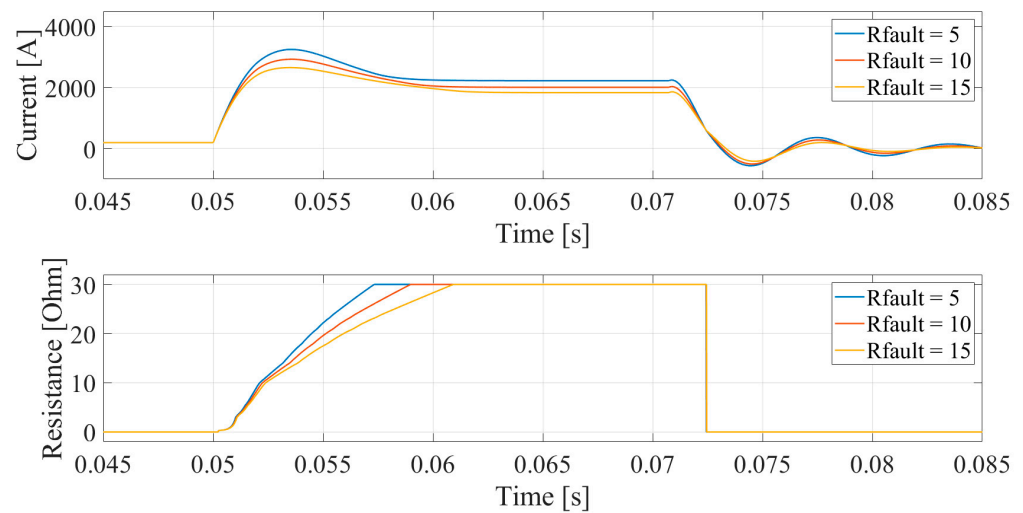**Figure 8.** RQ model analysis for different tape length values.

Figure 9. Influence of fault resistance in transition time of RQ model.

3.4. Magneto-Thermal Model

The magneto-thermal model depicted in Figure 4 is implemented in the test grid along with the thermal model of Section 2, Equations (13)–(17).

In this model, several parameters can be modulated. However, for the sake of simplicity, the parameters have been set in order to show a similar current-limiting response to the previous three models.

Figure 10 shows fault current, resistance evolution, voltage across the R-SFCL and M-DCCB along with temperature of the tape.

The magneto-thermal model shows the most realistic behavior of all presented models, where the nonlinear evolution of the resistance is precisely modeled. It is important to emphasize that this model is the only one where electrical variables have dependence with temperature. Once the fault is cleared, the R-SFCL device must cool down to come back to a superconducting state before the faulted line is reconnected.

Besides, the model has been evaluated for 5, 10, and 15 Ω fault resistances, as depicted in Figure 11. For larger fault resistances, the quenching is slowed down. It is important to remark that this behavior occurs with the RQ model but not with the first two simplified models.
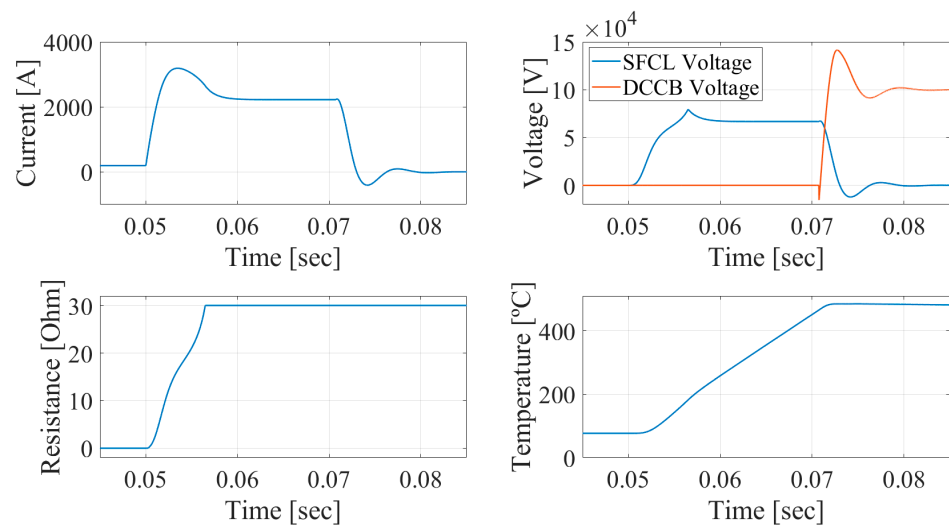
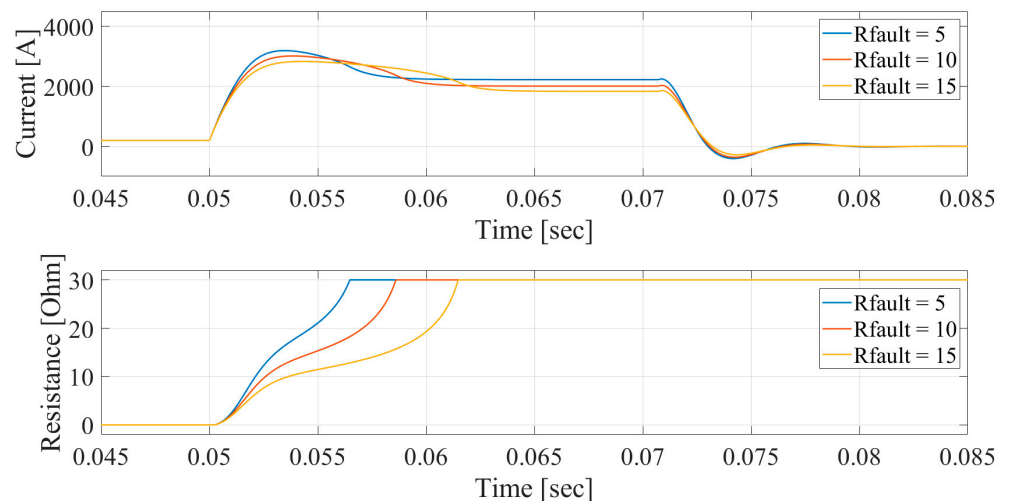**Figure 10.** Magneto-thermal model response.

Figure 11. Influence of fault resistance in transition time of magneto-thermal model.

The magneto-thermal model is the most accurate model, but it is also the most complex, computational cost demanding, and variable demanding model. However, if the configuration of the variables and their physical performance is well understood, the model can help with the design of the limiter.

3.5. Discussion

Along the previous subsections, the performance of four different types of R-SFCL models have been analyzed in the same system. Depending on the model settings and the model itself, the behavior of each model differs. In this section the performance of all models are encompassed in the same figure and their distinct response to critical current and fault resistance variations is emphasized.

Figure 12 shows fault current and resistance evolution of all models for a critical current value of 300 A (1.5 pu) and fault resistance value of 5 Ω. The main difference among the models is observed in the flux-flow state. It is appreciated that the RQ model shows a more realistic resistance shape evolution compared to the step and exponential model. Therefore, for this fault resistance and critical current values, the current evolution is equalized to the magneto-thermal model.
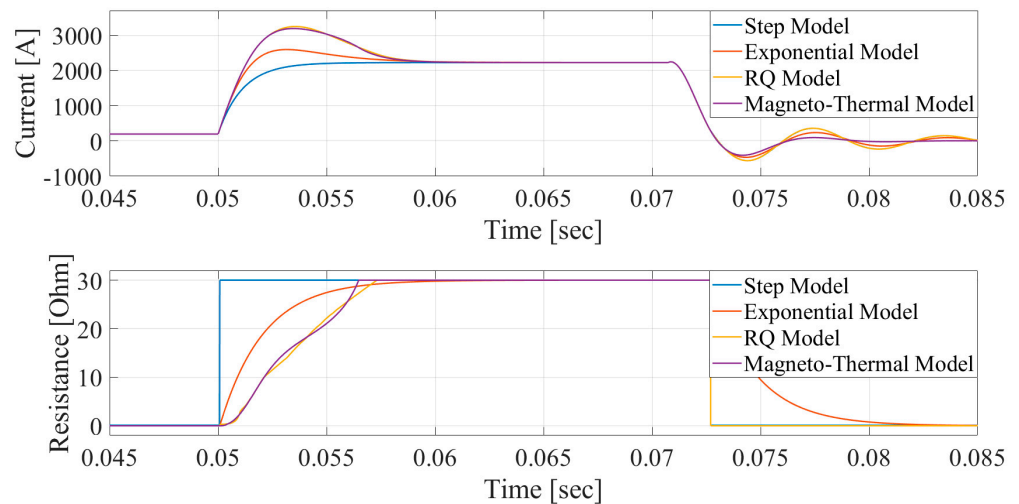
Figure 12. Model comparison for 300 A critical current and 5 Ω fault resistance.

Distinct behaviors for different fault resistances have been observed in the previous subsection. In consequence, Figure 13 shows all model responses for 300 A critical current and 15 Ω fault resistance values. It can be observed that fault resistance has an impact on the transition time for RQ and magneto-thermal models, whilst it does not for step and exponential models.
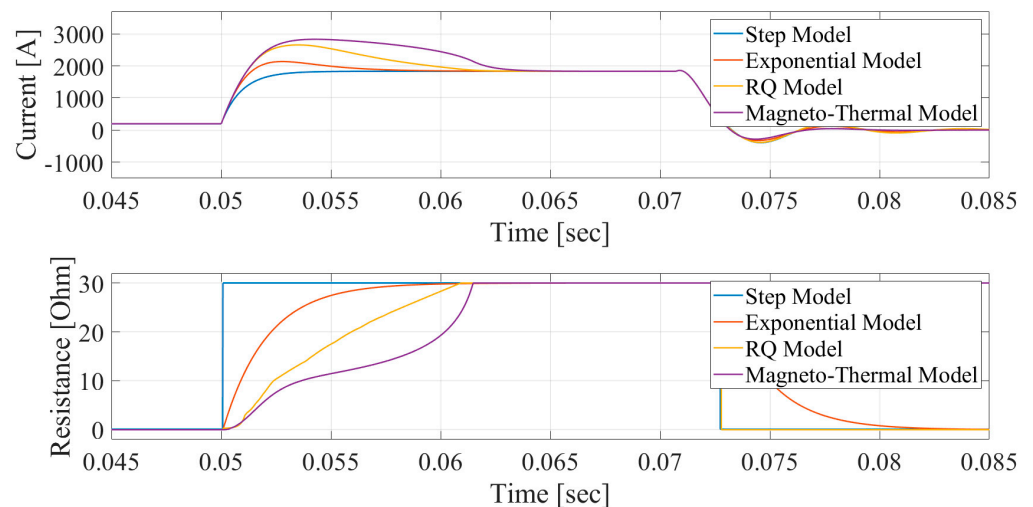

Figure 13. Model comparison for 300 A critical current and 15 Ω fault resistance.

This way, even though the final resistive value and steady state fault current are the same, the peak value will differ for distinct fault resistances, as appreciated in Figure 14.

Finally, critical current influence is evaluated. Figure 15 shows all model responses for 400 A (2 pu) critical current and 5 Ω fault resistance values. In the step, exponential and RQ models, large variations in the critical current have a small impact (similar peak current to the one depicted in Figure 12), whilst magneto-thermal model response shows a great dependence on the critical current.
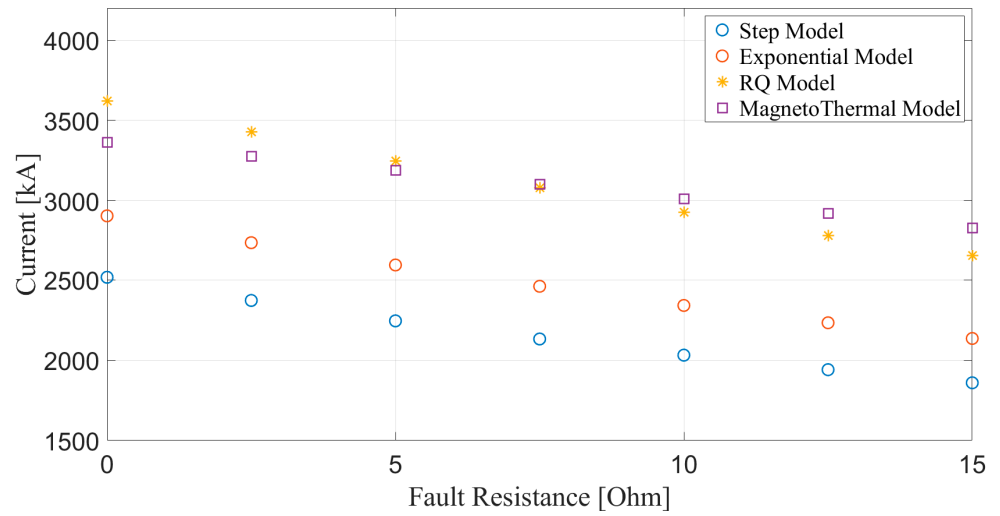
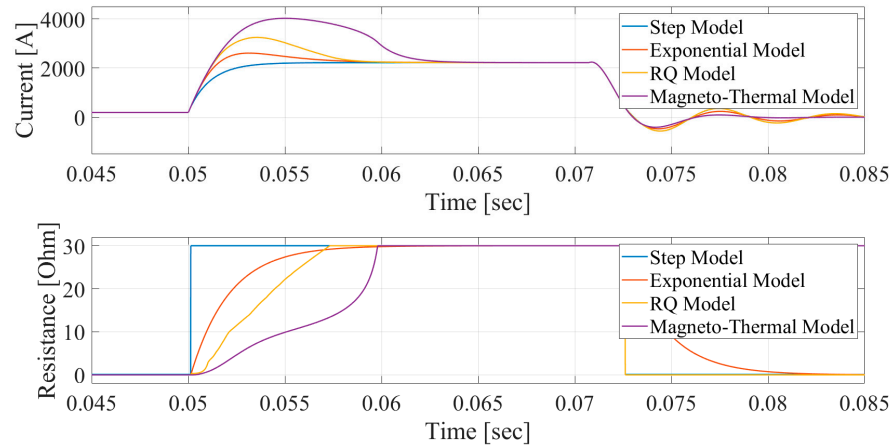**Figure 14.** Peak current comparison for different fault resistance values and 300 A critical current.

Figure 15. Model comparison for 400 A critical current and 5 Ω fault resistance.

Once again, even though the final R-SFCL resistance and steady state fault current value are the same, the peak value will differ for distinct critical current values, as shown in Figure 16.
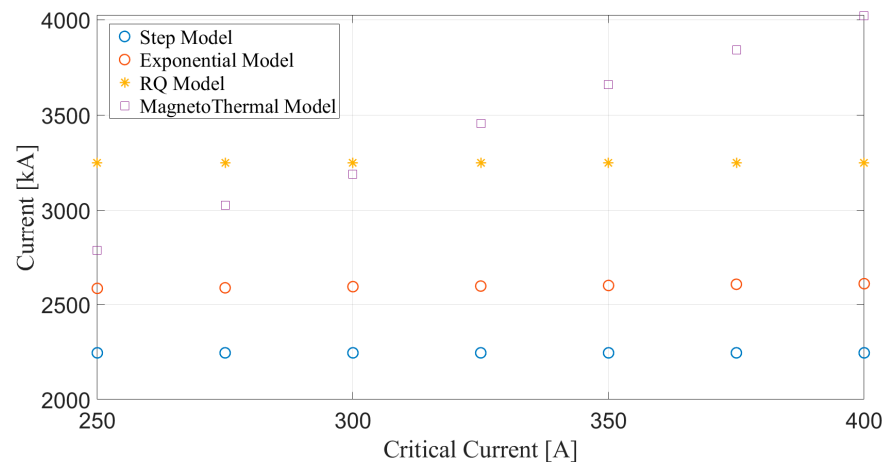

Figure 16. Peak current comparison for different critical current values and 5 Ω fault resistance.

To summarize, the complexity of the presented models increases in the order of appearance. The step model is extremely simple. However, it presents no flux-flow state. The exponential model presents a generally correct transition. The RQ model is not a complex model, though it shows a more precise response than the previous models due to its sensitivity to fault resistance. Finally, the thermo-electrical model is the most complex, most demanding in computational cost, and most accurate. In this model, electric parameters change with temperature, which differs from the remaining models where electric and thermal parameters are decoupled.

4. R-SFCL in a HVDC Grid

After evaluating the four models in a basic testbed with MATLAB/Simulink, the RQ model has been implemented in PSCAD/EMTDC and tested in the HVDC grid shown in Figure 17. The RQ model has been chosen for its simplicity but with more approximated behavior to the magneto-thermal model in terms of fault resistance dependency and resistance evolution curve.
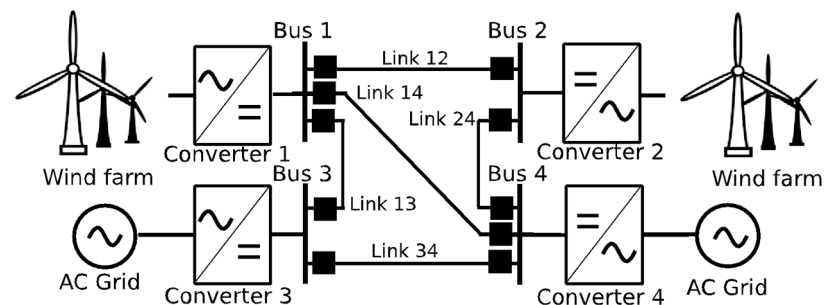

Figure 17. HVDC grid.

The HVDC grid is composed of four modular multilevel converters. Converters 1 and 2 are connected to offshore windfarms (PQ control) whilst converters 3 and 4 are connected to mainland grid (voltage control). Further information about the test grid is developed in [35]. Table 3 shows HVDC grid and converter parameters.

Table 3. HVDC grid parameters.

	Converter 1, 2, 3	Converter 4	Unit
Rated Power	900	1200	[MVA]
Rated DC voltage	±320	±320	[kV]
Rated DC Current	1.406	1.875	[kA]
IGBT Blocking Current	2.1 (1.5 pu)	2.1 (1.12 pu)	[kA]
AC Grid Voltage	400	400	[kV]

Five cables interconnect the converters, their lengths being 200 km (links 13 and 14), 150 km (link 24), and 100 km (link 12 and 34). At both terminals of each link, there is a 100 mH limiting inductor in series with the R-SFCL and an M-DCCB. The parameters of the M-DCCB (Figure 6) are shown in Table 2. The model settings of the implemented R-SFCL RQ model are shown in Table 4.

Table 4. RQ model settings for HVDC grid.

Variable	Value	Unit
Length	4	[km]
Resistance	80	[Ω]
Critical current	2	[kA]

Next, pole-to-pole and pole-to-ground faults at Link 12 just beside Bus 1 are analyzed to discuss the influence of the integration of the R-SFCL.

4.1. Pole-to-Pole Faults

In this section the performance of the RQ modelled R-SFCL is assured with highly demanding pole-to-pole faults in the HVDC grid. Pole-to-pole faults in HVDC systems are characterized by a large rise rate and final current value, as well as a severe voltage drop in the DC link, which theoretically drops to zero in case of solid faults.

Figure 18 shows the fault behavior of Converter 1 with and without R-SFCL when a solid pole-to-pole fault occurs in Link 12 beside Bus 1 at the instant t = 0.51 s. In the no R-SFCL scenario, Converter 1 feeds the fault with a large current value and DC voltage drops close to zero. However, when R-SFCL is integrated, it can be appreciated that the converter's current gets substantially limited and the voltage level is maintained as the R-SFCL quenches fast with a large enough value. Finally, the fault neutralization time of the M-DCCB is approximately at t = 0.514 s, and instants later the fault is cleared. Subsequently, the power flow and pre-fault variables reset after an oscillating transient period, enabling the continuity of the system.
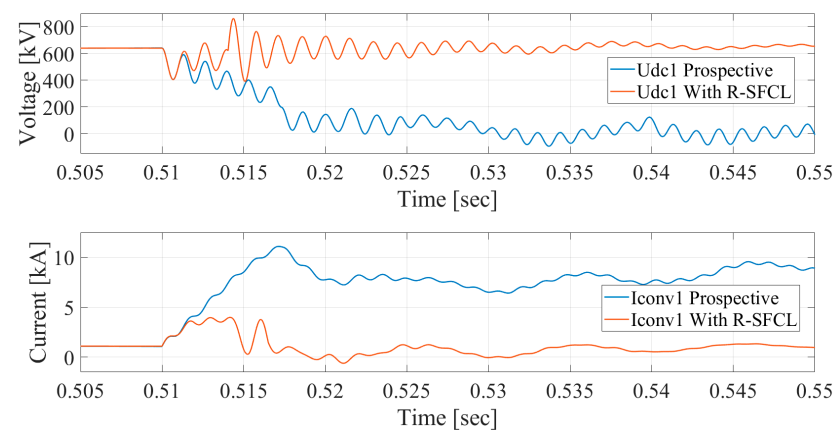

Figure 18. Converter 1 behavior with and without current limiter under pole-to-pole fault in Link 12 near Bus1.

Figure 19 shows the response of all converters' DC currents with and without R-SFCL under solid pole-to-pole fault scenario. Converters connected to the faulted link immediately withstand a high gradient current fault, whereas the travelling wave delays the response of most distant converters. Nevertheless, these converters are connected to AC grids. Therefore, their contribution to the fault current is large. Besides, with the R-SFCL a reduction of the fault current of is appreciated. Table 5 sums up the maximum current values of all converters and limiting factors, which is defined in Equation (18).

$$LF = \frac{I_{Prospective}}{I_{Limited}} \tag{18}$$

Table 5. Peak current and limiting factor comparison for pole-to-pole fault.

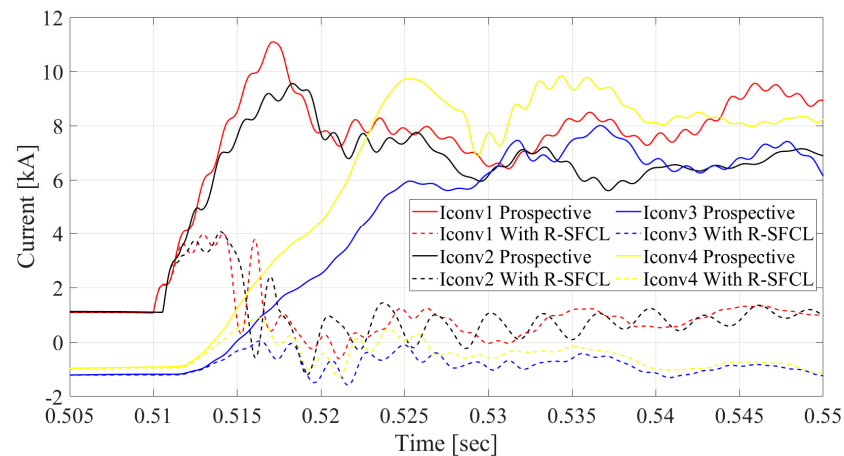|	Peak Current [kA]	Limited Peak Current [kA]	LF [-]
Converter 1	11.09	3.98	2.78
Converter 2	9.55	4.05	2.35
Converter 3	8	1.58	5.05
Converter 4	9.83	1.50	6.51

Figure 19. Converter's fault currents with and without current limiter under pole-to-pole fault condition.

With the integration of R-SFCLs, the peak currents, related to mechanical induced forces, and the final converter current, related to thermal stress, are drastically reduced.

According to the M-DCCB breaking capability reduction, Figure 20 shows current through the positive pole of Link 12 with a comparison between three scenarios: prospective fault current, fault current with M-DCCB, and the same scenario with the integration of R-SFCL. With the R-SFCL, the current breaking requirement of the M-DCCB drops from a peak fault current of 9.24 kA to 3.59 kA. In consequence, the rating of the M-DCCB is remarkably reduced. Therefore, it can be concluded that no fast trigger is needed to avoid high breaking capabilities.
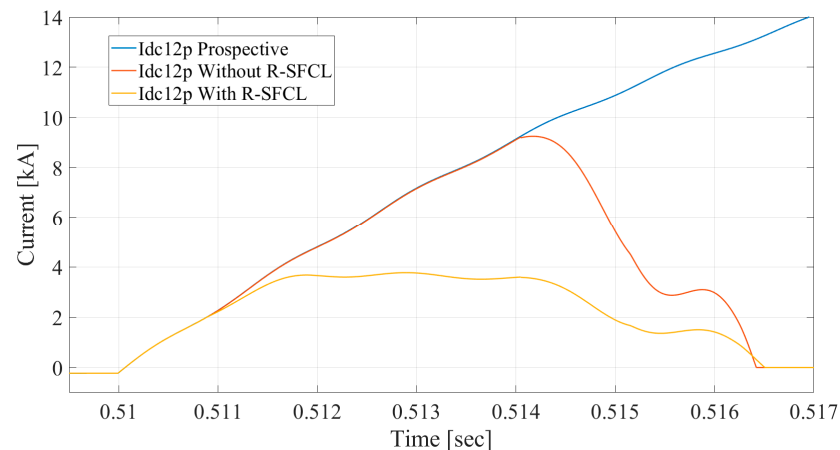

Figure 20. Link 12 positive pole fault currents for pole-to-pole fault, prospective, with M-DCCB, with M-DCCB and R-SFCL.

Finally, to further analyze the fault case scenario, Figure 21 shows peak currents for all converters with and without R-SFCL with a range of fault resistances from 0 Ω to 50 Ω. Higher fault resistances entail lower peak currents. Additionally, the considerable reduction in peak currents for all fault cases is remarkable.
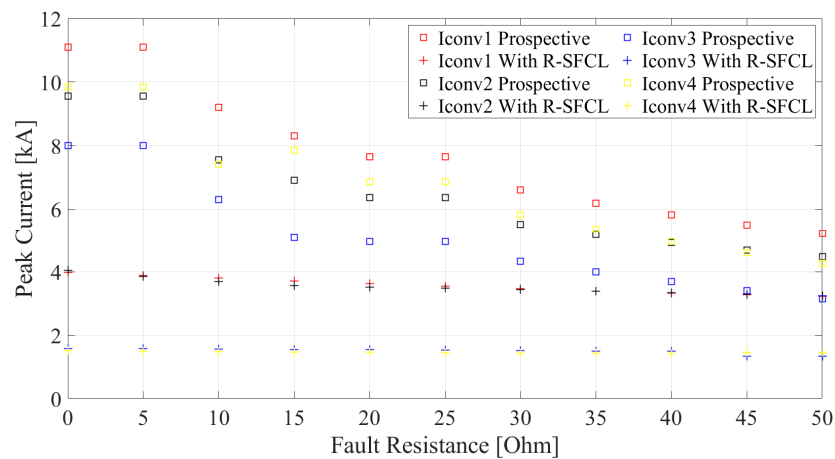
Figure 21. Prospective and limited converter fault peak currents for fault resistance swept between 0 and 50 Ω.

4.2. Pole-to-Ground Faults

Pole-to-ground faults differ radically from pole-to-pole faults in HVDC systems. In pole-to-ground faults there is a high initial peak current but there is no steady state fault current and the DC voltage at buses is maintained as pole-to-ground voltages get permanently unbalanced.

Figure 22 shows the behavior of converter 1 with and without R-SFCL under a pole-to-ground fault in the same location as pole-to-pole fault scenario. The initial transient current is limited and after the M-DCCB triggering, system variables convert to pre-fault values after an oscillating period, enabling continuity of the system operation.
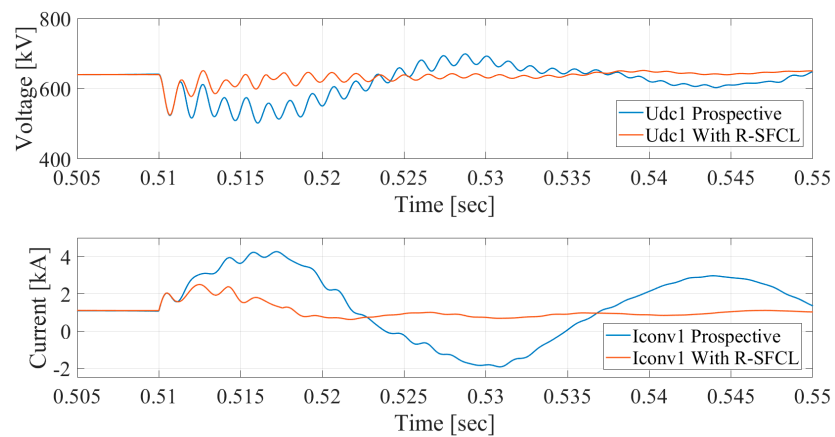

Figure 22. Converter 1 behavior with and without current limiter under pole-to-ground fault in Link 12 near Bus 1.

Prospective and peak currents for all converters with and without R-SFCL are shown in Figure 23. Converters 1 and 2, which are connected to the faulted link, provide the higher contribution to the fault currents. Limiting factors (Table 6) shows that current stress is limited.

According to the M-DCCB breaking capability reduction, the positive pole current of Link 12 is evaluated in a pole-to-ground fault encompassing the performance of the prospective current, the same case with the M-DCCB and finally, incorporating the R-SFCL and M-DCCB (Figure 24). In this last case, current requirement drops from 7.339 kA to 2.994 kA.
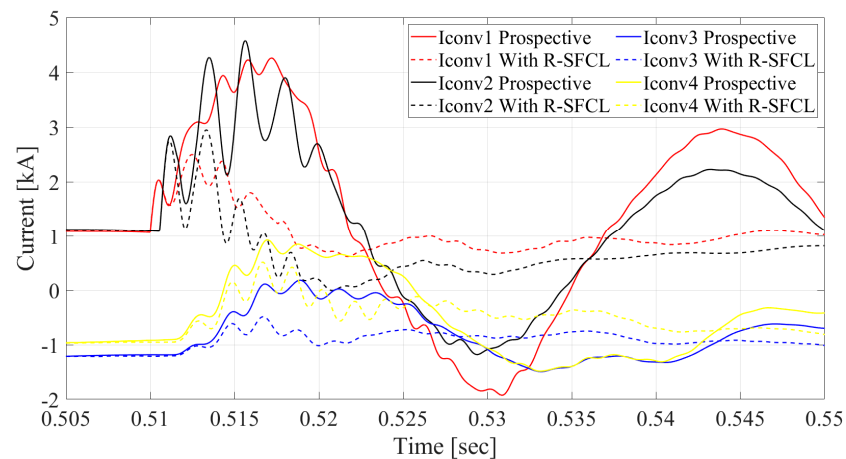
Figure 23. Converter fault currents with and without current limiter under pole-t- ground fault condition.

Table 6. Peak current and limiting factor comparison for pole-to-ground fault.

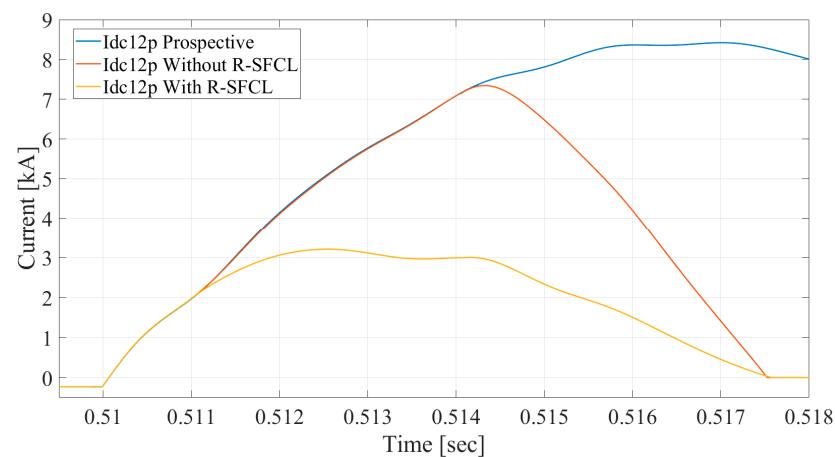|	Peak Current [kA]	Limited Peak Current [kA]	LF [-]
Converter 1	4.25	2.49	1.70
Converter 2	4.57	2.94	1.55
Converter 3	1.49	1.23	1.20
Converter 4	1.72	1.07	1.60

Figure 24. Link 12 positive pole fault current for pole-to-ground fault, prospective, with M-DCCB, with M-DCCB and R-SFCL.

4.3. Comparison

In this section, the results of the current study case (SC) are compared with those existing in the literature. Table 7 comprizes the main features of the considered papers. This way, the characteristics of the HVDC grid as well as the fault case scenario are included. Herein, PtP stands for pole-to-pole faults, and PtG for pole-to-ground faults. The employed DCCBs are hybrid DCCBs (Hyb) in most cases, while some authors employ mechanical DCCBs (Mec). The latters show larger fault clearing times. The models of the R–SFCLs are two level, exponential (Exp), look-up tables or magneto-thermal (MgTh) model. Some of the most relevant parameters of the models are included, i.e., the critical current (Ic) and the R-SFCL resistance. Finally, the current reduction as well as fault neutralisation time are depicted.

Table 7. Comparison with the existing literature.

Ref.	HVDC System (Fault Case)	DC CB	R-SFCL Model	Ic Rsfcl	I Red. (kA)	Fault Neutr. Time (ms)
[4]	4 terminal 60 kV 1.5 kA (PtP)	Hyb	2 state Exp MgTh	1.8 kA 30 Ω	From 8 to 4.5	6.5
[8]	3 terminal +160 kV 157 A	Hyb	2 state	0.18 kA 30 Ω	1.8	5
[9]	2 terminal 10 kV 10 MVA (PtP)	-	MgTh	0.5 to 4 Ω	From 12.9 to 7.5	10
[10]	4 terminal 320 kV 1.4/1.8 kA (PtP)	Hyb	Look up table	20 Ω	From 7.34 to 4.65	4
[11]	3 terminal 400 kV 500 MVA (PtG)	Mec	MgTh	3 kA	1.85	<30
[13]	VSC 320 kV 1 kA	-	Exp	10 Ω 20 Ω	7 and 5	5
[14]	2 terminal ±100 kV (PtP)	Hyb	Exp	13 Ω	From 6.93 to 4.58	-
[16]	320 kV 1.6 kA (PtG)	Hyb	Exp	20 Ω	From 13.01 to 9.56	8.6
SC	4-terminal 320 kV 1.4/1.8 kA (PtP)	Mec	Look up table	2 kA 80 Ω	From 11.09 to 3.98	25

5. Conclusions

This paper deals with the modelling of R-SFCLs in order to improve the performance of the protection system in HVDC grids. This way, the R-SFCL is connected in series with the DCCB, substantially reducing fault currents and, thus, the challenging rating of DCCBs. In the paper, four different models of R-SFCLs combined with an M-DCCB are analyzed and evaluated in a test grid. A representative variable range analysis has been performed and the different performances of each model have been discussed. Accordingly, the main conclusions are set out hereafter.

- The step model does not consider the dynamic performance in the transient period. Thus, it can be used for steady state analysis only.
- The exponential model is a simple model that emulates the transition phenomenon. However, it does not respond to changes in certain parameters, such as fault resistance and critical current.
- The RQ model is not complex, but still it characterizes the flux-flow state. The electric and thermal variables are decoupled, as in the preceding models. Besides, it is sensitive to fault resistance, which differentiates this model from the previous ones.
- The magneto-thermal model is the most complex, most demanding in computational cost, and most accurate model. The response shows the best resemblance to the phenomenon of all the considered models, given that electric parameters change with temperature and the realistic impact of critical current and fault resistance variations.
- The analysis of the RQ model with a M-DCCB in a HVDC grid shows an adequate performance in case of demanding faults. This way, fault currents decrease to a great extent which results in a large reduction of the converter stress and M-DCCB requirements. The power flow is restored faster and the transient stability of the system is upgraded. Therefore, the R-SFCL enables a reliable protection of the HVDC grid.

The results of the paper are restricted by the considered assumptions (homogeneous current density distribution). Further works are being carried out on the impact in the performance of HVDC grids protection of the design parameters and different internal device level phenomena (such as hot spots) using the magneto-thermal model.

Author Contributions: Conceptualization, methodology, and writing—review and editing: G.G., D.M.L. and A.E.; Software, validation, formal analysis, investigation and data curation: G.G.; Writing—

References

1. Bucher, M.K.; Franck, C.M. Fault Current Interruption in Multiterminal HVDC Networks. *IEEE Trans. Power Deliv.* **2016**, *31*, 87–95. [CrossRef]
2. Jovcic, D.; Tang, G.; Pang, H. Adopting Circuit Breakers for High-Voltage dc Networks: Appropriating the Vast Advantages of dc Transmission Grids. *IEEE Power Energy Mag.* **2019**, *17*, 82–93. [CrossRef]
3. CIGRÉ WG B4.52. In *HVDC Grid Feasibility Study*; Cigré: Paris, France, 2013.
4. Chang, B.; Cwikowski, O.; Pei, X.; Barnes, M.; Shuttleworth, R.; Smith, A.C. Impact of fault current limiter on VSC-HVDC DC protection. In Proceedings of the 12th IET International Conference on AC and DC Power Transmission (ACDC 2016), Beijing, China, 28–29 May 2016; pp. 1–6. [CrossRef]
5. Noe, M.; Steurer, M. High-temperature superconductor fault current limiters: Concepts, applications, and development status. *Supercond. Sci. Technol.* **2007**, *20*, R15–R29. [CrossRef]
6. Tixador, P. *Superconducting Fault Current Limiter. Innovation for the Electric Grids*; World Scientific Publishing: Singapore, 2019.
7. Moyzykh, M.; Gorbunova, D.; Ustyuzhanin, P.; Sotnikov, D.; Baburin, K.; Maklakov, A.; Magommedov, E.; Shumkov, A.; Telnova, A.; Shcherbakov, V.; et al. First Russian 220 kV Superconducting Fault Current Limiter (SFCL) For Application in City Grid. *IEEE Trans. Appl. Supercond.* **2021**, *31*, 1–7. [CrossRef]
8. Chen, Z.; Wang, Y.; Qiu, F.; Wang, S.; Zeng, R.; Wang, X. Comparative Analysis and Design of Inductive and Resistive SFCL for HB-MMC-HVDC Under DC Faults. In Proceedings of the 5th IEEE Conference on Energy Internet and Energy System Integration, Taiyuan, China, 22–24 October 2021. [CrossRef]
9. Li, B.; He, J. Studies on the Application of R-SFCL in the VSC-Based DC Distribution System. *IEEE Trans. Appl. Supercond.* **2016**, *26*, 1–5. [CrossRef]
10. Mokhberdoran, A.; Carvalho, A.; Silva, N.; Leite, H.; Carrapatoso, A. Application study of superconducting fault current limiters in meshed HVDC grids protected by fast protection relays. *Electr. Power Syst. Res.* **2017**, *143*, 292–302. [CrossRef]
11. Garcia WR, L.; Bertinato, A.; Tixador, P.; Raison, B.; Luscan, B. Protection strategy for multi-terminal high-voltage direct current grids using SFCLs at converter station output. *J. Eng.* **2018**, *15*, 1369–1374. [CrossRef]
12. Larruskain, D.M.; Iturregi, A.; Saldaña, G.; Apiñaniz, S. Performance of a superconducting breaker for the protection of HVDC grids. *IET Gener. Transm. Distrib.* **2020**, *14*, 997–1004.
13. Lin, Z.; Jin, J.; Yin, Q.; Liu, Y.; Xu, J.; Zeng, X. Study on Coordination of Resistive-Type Superconducting Fault Current Limiter and DC Circuit Breaker in HVDC system. In Proceedings of the 5th Asia Conference on Power and Electrical Engineering (ACPEE), Chengdu, China, 4–7 June 2020. [CrossRef]
14. Lee, H.; Asif, M.; Park, K.; Lee, B. Feasible Application Study of Several Types of Superconducting Fault Current Limiters in HVDC Grids. *IEEE Trans. Appl. Supercond.* **2018**, *28*, 1–5. [CrossRef]
15. Etxegarai, A.; Zamora, I.; Buigues, G.; Valverde, V.; Torres, E.; Eguia, P. Models for fault current limiters based on superconductor materials. *Renew. Energy Power Qual. J.* **2016**, *1*, 284–289. [CrossRef]
16. Singh, N.K.; Burt, G.M. *Improved Model of Superconducting Fault Current Limiter for Power System Dynamic Studies*; Technical Report; University of Strathclyde: Glasgow, UK, 2008.
17. Blair, S.M.; Booth, C.D.; Burt, G.M. Current–Time Characteristics of Resistive Superconducting Fault Current Limiters. *IEEE Trans. Appl.* **2012**, *22*, 5600205. [CrossRef]
18. Li, B.; Wang, C.; Ye, S.; Yang, S.; Xin, Y.; Wen, W.; Hong, W.; Sheng, C.; Zhong, L.; Duan, X.; et al. R-Q curve based evaluation method for current-limiting performance of DC R-SFCL in high voltage DC system. *Supercond. Sci. Technol.* **2020**, *33*, 084001. [CrossRef]
19. Seo, H.C.; Ko, Y.T.; Rhee, S.B.; Kim, C.H.; Aggarwal, R.K. A Novel Reclosing Algorithm Considering the Recovery Time of a Superconducting Fault Current Limiter in a Distribution System with Distributed Generation. In Proceedings of the 10th International Conference on Developments in Power System Protection, Manchester, UK, 29 March–1 April 2010.
20. Dul'kin, I.N.; Yevsin, D.V.; Fisher, L.M.; Ivanov, V.P.; Kalinov, A.V.; Sidorov, V.A. Modeling Thermal Process in a Resistive Element of a Fault Current Limiter. *IEEE Trans. Appl. Supercond.* **2008**, *18*, 7–13. [CrossRef]
21. Choi, Y.; Kim, D.; Yang, H.; Lee, B.; Jung, W. Cryocooled Cooling System for Superconducting Magnet. In Proceedings of the Proceedings of the 15th International Cryocooler Conference, Long Beach, CA, USA, 9–12 June 2009.
22. Zampa, A.; Tixador, P.; Badel, A. Effect of the Conductor Length on the Hot-Spot Regime for Resistive-Type Superconducting Fault Current Limiter Applications. *IEEE Trans. Appl. Supercond.* **2021**, *31*, 1–11. [CrossRef]

23. Sutherland, P.E. Analytical model of superconducting to normal transition of bulk high Tc superconductor BSCCO-2212. *IEEE Trans. Appl. Supercond.* **2006**, *16*, 43–48. [CrossRef]
24. Roy, F.; Dutoit, B.; Grilli, F.; Sirois, F. Magneto-Thermal Modeling of Second-Generation HTS for Resistive Fault Current Limiter Design Purposes. *IEEE Trans. Appl. Supercond.* **2008**, *18*, 29–35. [CrossRef]
25. Branco, P.J.C.; Almeida, M.E.; Dente, J.A. Proposal for an RMS thermoelectric model for a resistive-type superconducting fault current limiter (SFCL). *Electr. Power Syst. Res.* **2010**, *80*, 1229–1239. [CrossRef]
26. Shen, B.; Chen, Y.; Li, C.; Wang, S.; Chen, X. Superconducting fault current limiter (SFCL): Experiment and the simulation from finite-element method (FEM) to power/energy system software. *Energy* **2021**, *234*, 121251. [CrossRef]
27. Riva, N.; Sirois, F.; Lacroix, C.; De Sousa WT, B.; Dutoit, B.; Grilli, F. Resistivity of REBCO tapes in overcritical current regime: Impact on superconducting fault current limiter modeling. *Supercond. Sci. Technol.* **2020**, *33*, 114008. [CrossRef]
28. Shen, B.; Grilli, F.; Coombs, T. Overview of H-Formulation: A Versatile Tool for Modeling Electromagnetics in High-Temperature Superconductor Applications. *IEEE Access* **2020**, *8*, 100403–100414. [CrossRef]
29. Tan, X.; Ren, L.; Liang, S.; Tang, Y.; Xu, Y.; Shi, J.; Li, Z. Analysis of R-SFCL with Shunt Resistor in MMC-HVDC System Using Novel R-Q Method. *IEEE Trans. Appl. Supercond.* **2020**, *30*, 1–5. [CrossRef]
30. Langston, J.; Steurer, M.; Woodruff, S.; Baldwin, T.; Tang, J. A generic real-time computer Simulation model for Superconducting fault current limiters and its application in system protection studies. *IEEE Trans. Appl. Supercond.* **2005**, *15*, 2090–2093. [CrossRef]
31. Blair, S.M. The Analysis and Application of Resistive Superconducting Fault Current Limiters in Present and Future Power Systems. Master's Thesis, University of Strathclyde, Glasgow, UK, 2013.
32. Duron, J.; Grilli, F.; Antognazza, L.; Decroux, M.; Dutoit, B.; Fischer. Finite-element modelling of YBCO fault current limiter with temperature dependent parameters. *Supercond. Sci. Technol.* **2007**, *20*, 338–344. [CrossRef]
33. Liang, S.; Tang, Y.; Ren, L.; Xu, Y.; Wang, W.; Hu, Z.; Zhang, B.; Jiao, F. A novel simplified modeling method based on R–Q curve of resistive type SFCL in power systems. *Phys. C Supercond. Its Appl.* **2019**, *563*, 82–87. [CrossRef]
34. Kumar, M.A.; Babu, S.S.; Srikanth, N.V.; Chandrasekhar, Y. Performance of superconducting fault current limiter in offshore wind farm connected VSC based MTDC transmission system. In Proceedings of the 2015 IEEE Power and Energy Conference at Illinois (PECI), Champaign, IL, USA, 20–21 February 2015. [CrossRef]
35. Leterme, W.; Ahmed, N.; Beerten, J.; Ängquist, L.; Hertem, D.V.; Norrga, S. A new HVDC grid test system for HVDC grid dynamics and protection studies in EMT-type software. In Proceedings of the 11th IET International Conference on AC and DC Power Transmission, Birmingham, UK, 10–12 February 2015.